Int. J. Electrochem. Sci., 12 **(2017)** 9736 – 9746, doi: 10.20964/2017.10.35

International Journal of
ELECTROCHEMICAL
SCIENCE
www.electrochemsci.org

Preparation of Porous Carbon-Manganese Dioxide Nanocomposite for Sensitive Determination of Cadmium Ion

Hua Liu[1], *Xiaolin Yu*[1], *Huafeng Chen*[1] *and Yanhong Liu*[2,*]

[1] Department of Biomedical Engineering,Guangdong Pharmaceutical University, Guangzhou 510006, China
[2] Department of Endocrinology, The Second People's Hospital of Hengshui, Hengshui 053000, China
[*]E-mail: hongyanliu_ss@qq.com

Received: 29 June 2017 / *Accepted:* 6 August 2017 / *Published:* 12 September 2017

A cost-effective pyrolysis carbonization, together with a subsequent alkali activation, was performed for the preparation of activated porous carbons (APCs) with meso-/macropores and micropores. This was followed by electrodepositing manganese oxide nanostructures onto the as-prepared APC substrate with a constant anodic current. In addition, as studied by square-wave voltammetry (SWV) measurements, MnO_2-activated carbon (AC) was utilized for the detection of cadmium(II) (Cd(II)), where the metal ions accumulated on MnO_2-AC. Through the modification of the electrode surface and the optimization of relevant parameters, the behaviour of MnO_2-AC reached an optimum level in this study

Keywords: Activated porous carbon; Manganese oxide; Cadmium ion; Square wave voltammetry;

1. INTRODUCTION

The detection of heavy metal ions at trace levels has several applications in medicine, biology, process control, environmental determination, etc. It has been proposed that the neurotoxicity of cadmium, a toxicologically and environmentally noteworthy element, could lead to autism, vestibular dysfunction, impaired vision, speech difficulty, mental deterioration, hearing loss, etc. [1]. The detection of rather low concentrations of cadmium in a series of specimens (esp. water) is urgent, considering the increasing recognition of environmental cadmium toxicity and pollution. According to the World Health Organization (WHO), the guideline level of cadmium in drinking water is 1 μg/L. Due to the persistence and accumulative property in the biota and environment, cadmium has also been regarded as a highly dangerous element according to the Environmental Protection Agency (EPA). Additionally, considering the negative effects on human life, it is of great importance to quantify

extremely low levels of cadmium in clinical and environmental chemistry. Hence, the detection of cadmium at low levels has been investigated using diverse routes, including inductively coupled plasma (ICP) optical emission spectrometry, ICP mass spectrometry [2, 3], cold vapor atomic absorption spectroscopy (CVAAS) [4, 5] and neutron activation [6]. Unfortunately, most of these routes suffer from incompetence of on-site cadmium detection in most labs, high cost, time consumption, and multiple sample manipulations (involved the monitoring process). On the other hand, electrochemical detection has advantages over the abovementioned routes due to the fast response time, miniaturization, direct detection, low cost, ease of operation, etc. [7, 8]. Studies on the development and application of ion-selective electrodes in the detection of metal anionic and cationic species have been increasing, ascribed to the accuracy, rapidness, non-destructiveness, and low cost of the detection based on these electrodes [9-14].

Recently, activated carbons (ACs) have been increasingly applied in environmental fields, suggesting a steady increase in the global consumption of these materials. ACs can be prepared in various conformations, including powdered activated carbons (PACs), granular activated carbons (GACs) [15], activated carbon fibres (ACFs) [16], carbon monoliths and spherical activated carbons, considering the importance of the morphology of the ACs in the real application. Compared with powdered and granular ACs, spherical ACs have gained substantially increased attention due to their distinct characteristics, including controllable pore size distribution, high micropore volume, high bulk density, low pressure drop, desirable packaging, excellent fluidity, smooth surface, low ash content, high purity, remarkable adsorption performance, high mechanical strength, and high wear resistance [17]. Due to the abovementioned merits, spherical ACs have gained application in several fields, including catalyst supporting, blood purification in chemical protective clothing and sensing. In addition, this type of AC has been recognized as a potential candidate for a large number of adsorption processes, either in solution or in the gas phase. Based on the aforementioned results, an intense study was performed to prepare this type of AC with an optimization of different parameters.

In addition, growing attention has been paid to the development of cost-effective transition metal oxides, such as TiO_2, VO_x, Fe_3O_4, NiO, Co_3O_4, and MnO_2 [18-23]. Due to its environmental friendliness and inexpensiveness, manganese oxide has gained increasing attention. As a manganese oxide with the highest stability among manganese oxides, manganese dioxide exhibits remarkable chemical and physical features under ambient conditions.

Since electrochemical deposition can control the structure and thickness of deposited materials through the alteration of some parameters (temperature, electrodeposition voltage or current, electrolyte, etc.), this strategy is an excellent route to fabricate MnO_2 nanostructures. To prepare activated carbons, paulownia flower was used as a precursor, where high-temperature carbonization was performed along with the subsequent alkali activation. This was followed by electrodepositing manganese oxide nanostructures onto the as-prepared APC substrate with a constant anodic current. Cd(II) ions were electrochemically detected using the electrode after modification by MnO_2-AC. The highly sensitive, stable and fast detection of Cd(II) was greatly enhanced after adding the MnO_2-AC hybrid. The behaviour of the newly developed technique for the stripping detection of Cd(II) was studied in detail.

2. EXPERIMENTS

2.1. Chemicals and activated porous carbon synthesis

All test chemicals were of analytical grade and used without additional purification. Mature paulownia flower was collected after falling from paulownia trees. After rinsing using deionized water and naturally drying, the paulownia flower was kept under pyrolysis for 120 min at 800 °C in a nitrogen atmosphere to afford activated carbon. This was followed by mixing KOH with the above activated carbon, and the mass ratio of KOH to activated carbon was 2, 3, or 4. Pores were formed after further pyrolyzing the as-prepared mixture for 60 min at 800 °C under a nitrogen atmosphere. Note that the afforded product is referred to as AC_n (n = 2, 3, or 4, as stated above). This product was cooled naturally, followed by copious washing using 1 M HCl and deionized water to obtained a neutral pH state.

2.2. Electrodeposition of manganese oxide

A slurry that contained a polytetrafluoroethylene binder (5 mw%), acetylene black (10 mw%) and the active material (85 mw%) was spread onto a clean stainless-steel mesh collector to prepare the test AC electrodes. An anodic current (0.5 mA/cm^2) was applied to a mixture of sodium sulphate and manganese acetate (0.1 M for each) at ambient temperature for 0.5 min for the deposition of manganese oxide nanostructures onto the AC_n substrate (denoted as MnO_2-AC_n). The obtained MnO_2-AC_n electrode was electrodeposited, followed by rinsing several times using deionized water and air annealing for 60 min at 300 °C.

2.3. Cd ions determination

Cd ions were detected by immersing the as-prepared MnO_2-AC_n electrode into a magnetically stirred solution containing Cd(II) (20 ml) at the open circuit potential. This was followed by electrode removal, rinsing, and drying using adsorbent paper. Afterwards, the as-prepared electrode was introduced into a KNO_3 solution (0.2 M). A potential of −1.0 V (*vs.* Ag/AgCl reference electrode) was applied in the still solution for 10 s. Upon the expiration of the reduction time, square-wave voltammetry (SWV) with a positive-sweeping potential scan (−1.0 to −0.5 V) was applied at 50 mV/s (step potential, 25 mV) to obtain a second order derivative scan voltammogram, where the amplitude, duration and scan rate were 5 mV, 5 s and 1 mV/s, respectively. All measurements were carried out at ambient temperature.

2.4. Electrochemical impedance spectroscopy measurement

The abovementioned three-electrode geometry was used for electrochemical impedance spectroscopy (EIS) experiments before and after the accumulation step. After immersion in non-de-aerated solutions for 0.5 h, impedance spectra were recorded in the frequency range of 100 kHz to 10

mHz with 10 points per decade at a potential of 0 V. The system was perturbed by a sine wave with a 10 mV amplitude.

3. RESULTS AND DISCUSSION

As a conventional medical herb, paulownia flower possesses efficient antiphlogistic and bacteriostatic efficacies derived from the steroids, terpenoids, sugar esters, glucosides, flavonoids, and anthraquinones components enwrapped in the thick cell walls [24]. Carbon material was obtained by converting the abovementioned organics by a pyrolysis treatment. All specimens showed a broad and irrelevant diffraction peak at 26° associated with the (200) facet reflection, as indicated in the XRD profile of AC_n in Fig. 1A. This indicated the carbonization and the low graphitization phase of the test specimen. We also observed a peak associated with the (101) facet that suggested crystallinity via activation at a higher temperature. Since the entire crystallinity was low, this observation was rather important. Note that the crystallinity enhancement resulted in a further increased conductivity, which was necessary for the active electrode material to be considered a supercapacitor. At the low-angle region for AC_n, an enhanced baseline was observed, suggesting that rich micropores existed in the carbon framework. This result suggested that the alkaline treatment led to an enhancement in the porous texture, along with the enhanced crystallinity. MnO_2-AC_n was characterized via XRD (Fig. 1B), with the pattern of MnO_2-AC_n comparable to that of α-MnO_2 (JCPDS 44-0141). Other phases (i.e., γ-MnO_2) possibly existed; however, the main phase was attributed to α-MnO_2. Based on Scherrer's equation, the average grain size of the CF-deposited manganese oxide was calculated as 10 nm. The performance of the newly developed cadmium-ion sensor is based on the accumulation of cadmium from an aqueous solution onto the surface of the modified electrode [25].

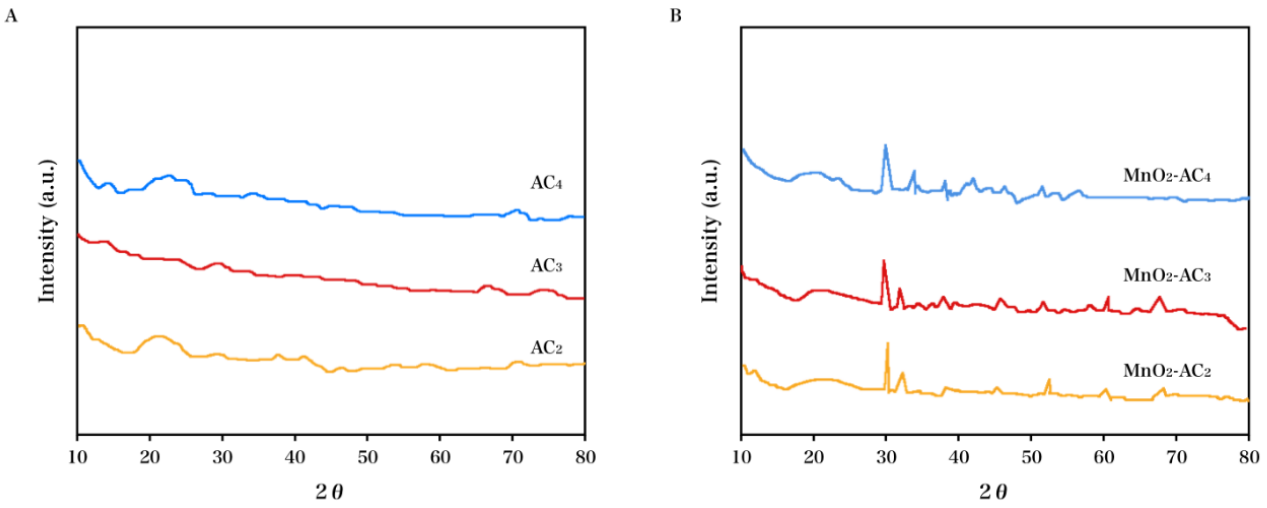

Figure 1. XRD patterns of (A) AC_n and (B) MnO_2-AC_n.

The combined type I/IV isotherm based on the IUPAC classification dominated all the nitrogen sorption isotherms of MnO_2- AC_n, where a unique and rapid adsorption at a relative pressure below 0.1 and a weak but observable type II triangular hysteresis loop at a relative pressure over 0.4 were observed, as indicated in Fig. 2. These results suggested that overwhelming micropores were present, as well as a low fraction of interconnected mesopores with a narrow orifice and large inner cavity, corresponding to the morphological features. Furthermore, the amount of adsorption slightly increased at a relative pressure close to 1, indicating a limited fraction of macropores in the specimens. This versatile porous structure could be well applied as an active electrode material for a supercapacitor due to its meso-/macropores and micropores. Specifically, the interconnected meso-/macropores functioned as large electrolyte ion diffusion pathways along varying directions with less geometric obstruction and short distances.

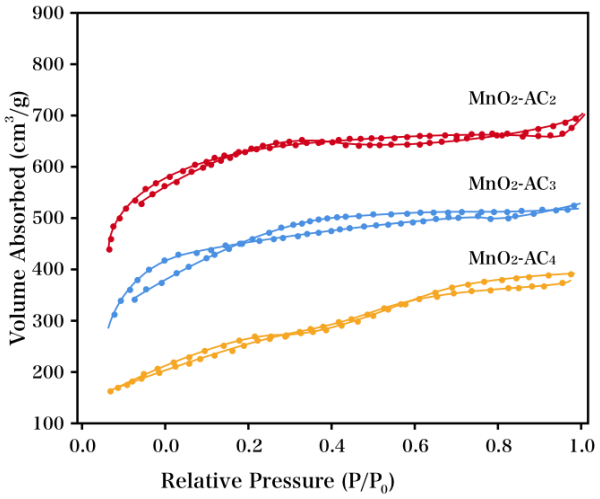

Figure 2. N_2 sorption isotherms of MnO_2-AC_2, MnO_2-AC_3 and MnO_2-AC_4.

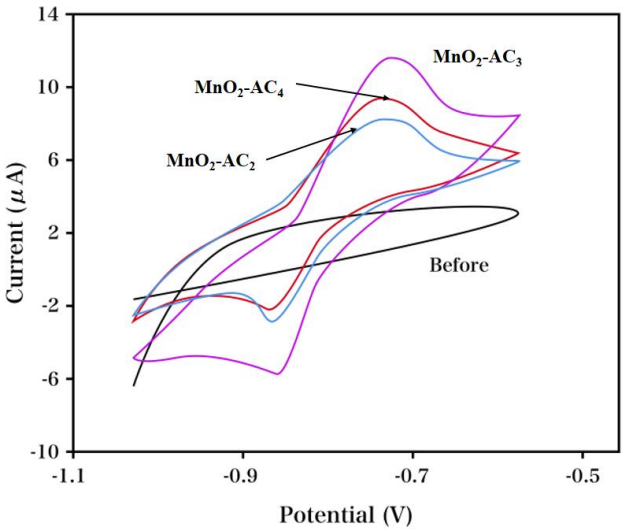

Figure 3. CV of the undecorated electrode, MnO_2-AC_2, MnO_2-AC_3 and MnO_2-AC_4 with Cd(II) and after incubation with Cd(II) species over 30 min in KNO_3 (0.2 M, pH 4).

In addition, a considerably accessible surface area was formed due to the micropores, which was beneficial for electrolyte ion accumulation. MnO_2-AC_2, MnO_2-AC_3 and MnO_2-AC_4 exhibited BET surface areas of *ca.* 1006, 1159, and 1471 m^2/g, respectively. These result showed higher values than those of recently reported biomass carbon [26], nitrogen-doped graphene aerogels [27], a spongy nitrogen-doped activated carbonaceous hybrid [28] and nitrogen-functionalized microporous carbon nanoparticles [29].

The undecorated electrode, MnO_2-AC_2, MnO_2-AC_3 and MnO_2-AC_4 towards the detection of Cd(II) were characterized via cyclic voltammograms (CVs) (Fig. 3). A relatively small peak current was observed (potential range, −1.0 V to −0.5 V), ascribed to the Cd(II)/Cd(0) redox couple. MnO_2-AC exhibited a more pronounced Cd(II)/Cd(0) redox reaction. As shown in these results, cadmium pre-concentration at the electrode could be enhanced by MnO_2-AC, which also promoted the detection sensitivity towards cadmium. The peak current enhancement can be also ascribed from the excellent electroconductivity of MnO_2 [30]. The current response to the Cd(II)/Cd(0) redox was the highest at MnO_2-AC_3, as shown in the cyclic voltammogram (CV). Hence, MnO_2-AC_3 was selected for the following measurements.

As shown in Fig. 4, EIS measurements were performed to study the performance of MnO_2-AC_3 before and after accumulation. The charge-transfer resistance (R_{tc}) values were obtained from the difference in impedance at higher and lower frequencies. We also assessed the double-layer capacitance (C_{dl}) and the frequency where the maximum imaginary component of the impedance ($-Z_{max}$) was obtained.

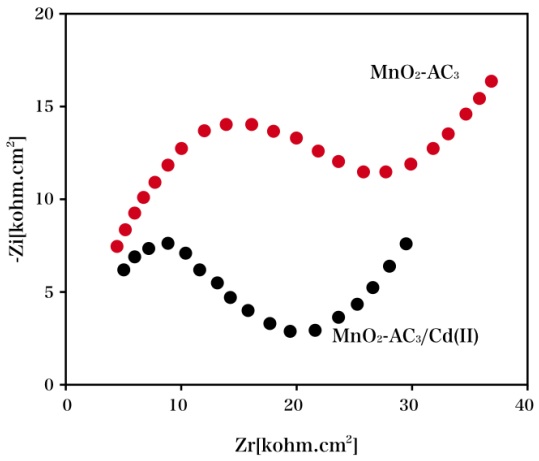

Figure 4. Impedance spectra of MnO_2-AC_3 and MnO_2-AC_3/Cd(II) at 0 V in 0.1 M KCl + 5 mM $[Fe(CN)_6]^{3/4}$. The frequency range: 0.1 Hz - 100 kHz; amplitude of the sine voltage signal: 5 mV.

The impedance spectra were recorded in a frequency range of 100 kHz - 10 mHz at 0 V. The C_{dl} and R_t values derived from the Nyquist plots are presented in Table 1. Herein, a steric hindrance effect exerted on $[Fe(CN)_6]^{-3/-4}$ electron transfer was found by the electrode. Therefore, we can use the CV response to calculate the surface density of MnO_2-AC_3,

$$\Gamma_{MB} = \frac{Q}{nFA} N_A$$

$$\Gamma_{DNA} = \Gamma_{MB}$$

where Γ_{MB} is the surface density (in molecules/cm^2) of MnO_2-AC_3, Q is the integrated charge of the cathodic peak, n is the number of electrons involved in the redox reaction, F is Faraday's constant, N_A is Avogadro's number, and A is the electrode area (0.211 cm^2).

After the addition of accumulated Cd(II), a decrease in the R_t value was observed, as shown in the impedance results. The values of the double-layer capacitance also decreased to a minimal degree after the addition of Cd(II), and an increase in the value of C_{dl} was observed. The C_{dl} increased due to Cd(II) accumulating on the surface of the electrode.

Table 1. Electrical parameters recorded in the impedance spectra for the MnO_2-AC_3/Cd(II) solution interfaces in KNO_3 (0.2 M).

	Re (Ω/cm^2)	Rct (Ω/cm^2)	Cdl (pF/cm^2)
MnO_2-AC_3	1654	27800	235.5
MnO_2-AC_3/Cd(II)	693	15200	2298.6

The change of the anodic peak current with the accumulation time is shown in Fig. 5. As the accumulation time was prolonged, an increase in the peak current was observed, suggesting that Cd(II) adsorption increased with the prolonged accumulation time before reaching adsorptive equilibrium, which then led to more considerable peak current. The pre-concentration time was optimized as 25 min for the following measurements.

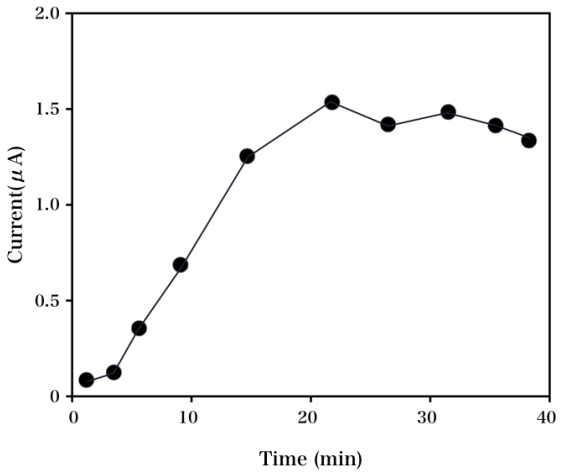

Figure 5. Effect of the accumulation time on the charge transfer of Cd(II) (1.5 μM) in KNO_3 (0.2 M, pH 4).

As displayed in Fig. 6, the effect of the pH value (1.8 - 9.5) on the SWV response of MnO_2-AC_3 was investigated in a solution that contained cadmium (1.5 μM). The maximal response was observed at 5.0, and the optimal pH range was 4.5 - 6.0. As the reduction peaks decreased, a decrease

in the sensitivity was observed in acidic solution due to the slow dissolution of kaolin, along with the loss of adsorption capacity. Hence, the optimal pH was selected as 5.0 for the following experiments.

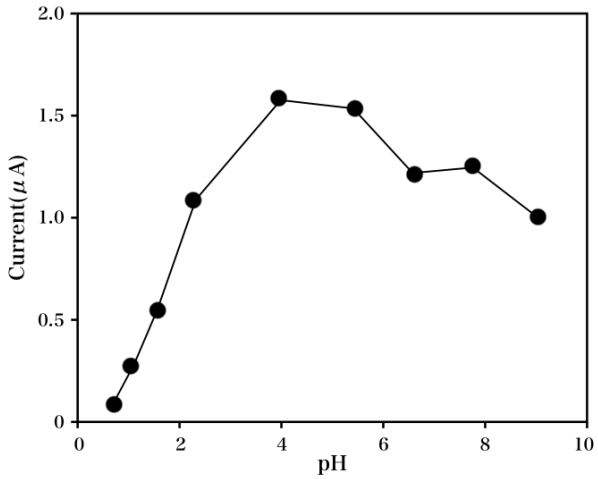

Figure 6. Effect of the pH value on the oxidation peak (SWV) for Cd(II) (1.5 μM) in KNO_3 (0.2 M).

The anodic peak currents of Cd(II) with varying concentrations of Cd(II) are displayed in Fig. 7. Under optimal conditions, a linear relationship between the concentration of Cd(II) and its peak current was found based on the regression equation, and the linear dynamic range was 50 nM - 8 μM. In addition, the limit of detection was calculated as 12 μM (S/N=3). For seven repeated experiments for a solution that contained 5.1 μM Cd(II), the relative standard deviation obtained was 3.28%. Additionally, we compared this electrode with some other different modified electrodes for the simultaneous determination of Cd(II), as summarized in Table 2.

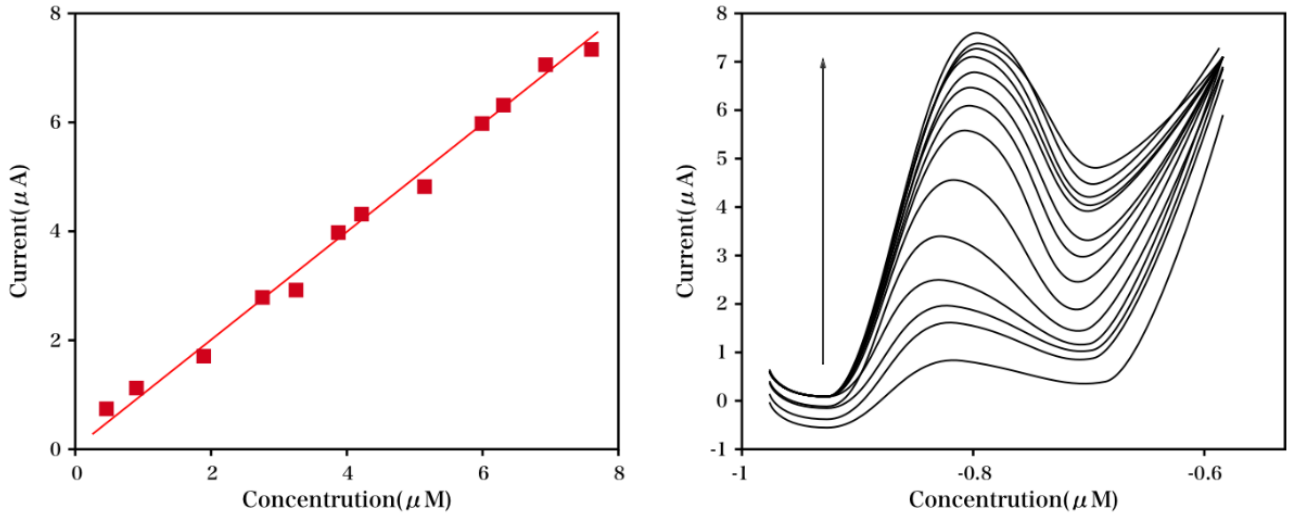

Figure 7. Square-wave voltammograms (SWVs) at MnO_2-AC_3 for the detection of Cd(II) in KNO_3 (0.2 M, amplitude: 5 mV, duration: 5 s, scan rate: mV/s).

During the pre-concentration process, other test ions were introduced to the specimen solution containing cadmium to investigate the selectivity of our proposed route for cadmium detection. The interfering effects of several metal ions on Cd(II) detection were investigated by immersing MnO_2-AC_3 into a mixture that contained 5.0 μM Hg(II), 5.0 μM Pb(II), 5.0 μM Ag(I), 5.0 μM Cu(II), and 5.0 μM Cd(II). An oxidation signal was observed due to Cd(II) at −0.85 V without interfering effects recorded in the case of the present study, as displayed in the voltammogram (Fig. 8). Clean separation was observed between the potential peaks, suggesting that Cd(II) could be detected with no interfering effects from the other common heavy metals.

The developed protocol was applied for monitoring Cd^{2+} ions in environmental and industrial effluents (Table 3). In the industrial effluent, approximately 1.5 μM Cd^{2+} was detected, and in lake water, approximately 0.5 μM Cd^{2+} was detected. Then, this sample was spiked with a known amount of the abovementioned metal ions and analysed. The recoveries were found to be more than 97%. The results obtained with the proposed method were validated by the AAS method (Table 2).

Table 2. Detection limits (DL) and linear ranges (LR) of different modified electrodes for determination of Cd(II).

Electrode	DL (μM)	LR (μM)	Reference
Carbon nanotube/GPE	0.1-5	0.0483	[31]
1,9-nonanedithiol on gold	0.05	0.1-10	[32]
SWASV	0.16	0.2-5	[33]
MWCNT- Schiff base	0.045	0.2-10	[34]
MnO_2-AC_3	0.0051	0.05-8	This work

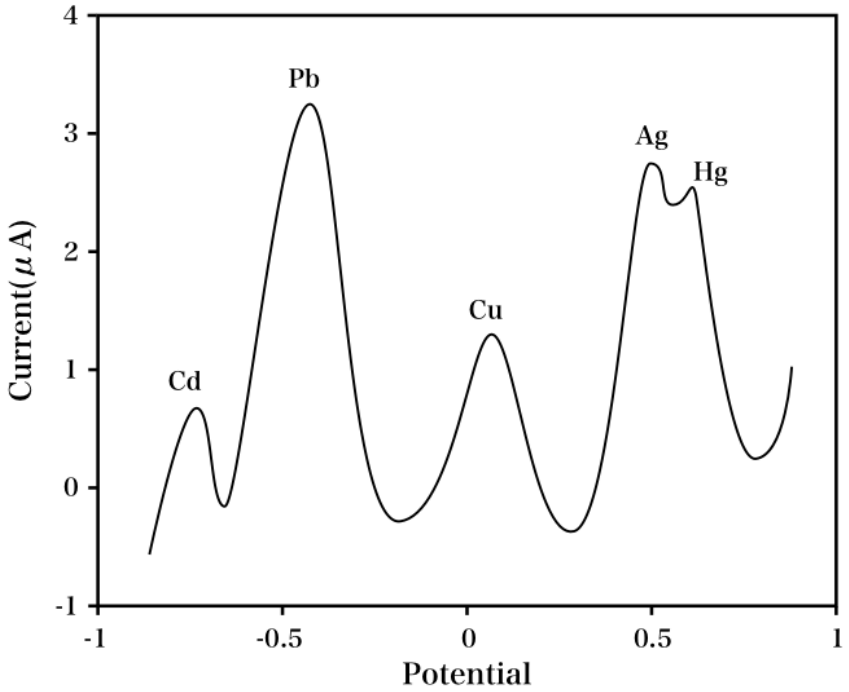

Figure 8. CV after exposure to a solution that contained Pb(II), Hg(II), Cu(II), Ag(I), and Cd(II).

Table 3. Determination of Cd^{2+} in environmental and industrial effluents (n = 3)

	MnO_2-AC_3 (μM)	AAS (μM)	Added (μM)	MnO_2-AC_3 (μM)	AAS (μM)	Recovery (%)MnO_2-AC_3	RSD (%)	Recovery (%) AAS
Industrial effluent	1.533	1.481	0.5	2.023	1.997	99.51	2.74	98.23
Lake water	0.512	0.513	0.5	1.024	1.017	101.16	3.05	100.49

4. CONCLUSIONS

In this work, Cd(II) was detected based on a hybrid film of MnO_2-AC_3. In addition, the MnO_2-AC_3 electrode has the potential of being used as an excellent sensor for the detection of heavy metals due to its desirable sensitivity. Furthermore, our proposed electrode proved to be highly reproducible.

ACKNOWLEDGEMENT
This work was supported by grants from The Science and Technology Plan of Guangdong Province (Grant No.2012B031000018) and 2017 research project from College of Medical Information Engineering of Guangdong Pharmaceutical University.

References

1. E. Beinrohr, M. Čakrt, J. Dzurov, L. Jurica and J.A.C. Broekaert, *Electroanalysis*, 11 (2015) 1137.
2. Y. Yamagishi, S. Furukawa, A. Tanaka, Y. Kobayashi and A. Sugiyama, *Journal of Toxicologic Pathology*, 29 (2016) 279.
3. R. Thompson and S. Christopher, *Analytical Methods*, 5 (2013) 1346.
4. J. Manzoori, H. Abdolmohammad-Zadeh and M. Amjadi, *Talanta*, 71 (2007) 582.
5. R. Moghaddam, A. Shabani, S. Dadfarnia and N. Baghban, *Journal of the Brazilian Chemical Society*, 25 (2014) 1975.
6. N. Zaim, C. Dogan and Z. Camtakan, *Journal of Applied Spectroscopy*, 83 (2016) 271.
7. M. Barciela, *Microchemical Journal*, 114 (2014) 106.
8. Z. Wang, H. Wang, Z. Zhang, X. Yang and G. Liu, *Electrochimica Acta*, 120 (2014) 140.
9. A. Sorbo, A. Turco, M. Gregorio and L. Ciaralli, *Food Control*, 44 (2014) 159.
10. J. Pérez-Outeiral, E. Millán and R. Garcia-Arrona, *Journal of Spectroscopy*, 2014 (2014) 1.
11. Q. Liu, K. Wang, J. Huan, G. Zhu, J. Qian, H. Mao and J. Cai, *The Analyst*, 139 (2014) 2912.
12. M. Junior, L.O. Silva, D. Leão and S. Ferreira, *Food Chemistry*, 160 (2014) 209.
13. A. Afkhami, M. Soltani-Shahrivar, H. Ghaedi and T. Madrakian, *Electroanalysis*, 28 (2015) 296.
14. Y. Wang, Y. Dong, J. Zhang, C. Li, J. Li and J. Ma, *Chemistry Letters*, 42 (2014) 153.
15. O. Hamdaoui and E. Naffrechoux, *J. Hazard. Mater.*, 147 (2007) 381.
16. I. Mochida, Y. Korai, M. Shirahama, S. Kawano, T. Hada, Y. Seo, M. Yoshikawa and A. Yasutake, *Carbon*, 38 (2013) 227.
17. Q.S. Liu, Z. Tong, W. Peng, J. Jiang and L. Nan, *Chem. Eng. J.*, 157 (2010) 348.
18. H. Hu, Q. Lin, A. Muhammad and B. Zhu, *Journal of Power Sources*, 286 (2015) 388.

19. S. Gowda, D. Dees, A. Jansen and K. Gallagher, *Journal of the Electrochemical Society*, 162 (2015) A1374.
20. D. Abraham, D. Dees, W. Lu, K. Gallagher, M. Bettge and A. Jansen, *Journal of the Electrochemical Society*, 162 (2015) A559.
21. W. Deng, X. Ji, Q. Chen and C. Banks, *Rsc Advances*, 43 (2015) 1171.
22. R. Clément, P. Bruce and C. Grey, *Journal of the Electrochemical Society*, 162 (2015) 2589.
23. M. Park, J. Kim, K. Kim, J. Lee, J. Kim and Y. Yamauchi, *Physical Chemistry Chemical Physics Pccp*, 17 (2015) 30963.
24. X. Li, P. Zhang, W. Duan, D. Zhang and C. Li, *Journal of Chinese Medicinal Materials*, 32 (2009) 1227.
25. M. El Mhammedi, M. Achak, M. Hbid, M. Bakasse, T. Hbid and A. Chtaini, *J. Hazard. Mater.*, 170 (2009) 590.
26. Awitdrus, M. Deraman, I. Talib, R. Farma, R. Omar, M. Ishak, E. Taer, B. Dolah, N. Basri and N. Nor, 1656 (2015) 11.
27. Z. Sui, Y. Meng, P. Xiao, Z. Zhao, Z. Wei and B. Han, *ACS Applied Materials & Interfaces*, 7 (2015) 1431.
28. S. Gharehkhani, S. Shirazi, S. Jahromi, M. Sookhakian, S. Baradaran, H. Yarmand, A. Oshkour, S. Kazi and J. Wan, *Rsc Advances*, 5 (2015) 40505.
29. Y. Zhao, M. Liu, X. Deng, L. Miao, P. Tripathi, X. Ma, D. Zhu, Z. Xu, Z. Hao and L. Gan, *Electrochimica Acta*, 153 (2015) 448.
30. J. Xu, H. Yu, Y. Hu, M. Chen and S. Shao, *Biosensors and Bioelectronics*, 75 (2016) 1.
31. L. Pikna, M. Heželová and Z. Kováčová, *Journal of Environmental Science & Health Part A Toxic/hazardous Substances & Environmental Engineering*, 50 (2015) 874.
32. E. Malel, J.K. Sinha, I. Zawisza, G. Wittstock and D. Mandler, *Electrochimica Acta*, 53 (2008) 6753.
33. V. Meucci, S. Laschi, M. Minunni, C. Pretti, L. Intorre, G. Soldani and M. Mascini, *Talanta*, 77 (2009) 1143.
34. A. Afkhami, H. Ghaedi, T. Madrakian and M. Rezaeivala, *Electrochimica Acta*, 89 (2013) 377.

© 2017 The Authors. Published by ESG (www.electrochemsci.org). This article is an open access article distributed under the terms and conditions of the Creative Commons Attribution license (http://creativecommons.org/licenses/by/4.0/).